Journal of Marine Research, 76, 139–161, 2018

Lagrangian dispersion characteristics in the Western Mediterranean

by Maher Bouzaiene[1,2], Milena Menna[3], Pierre-Marie Poulain[3,4] and Dalila Elhmaidi[1]

ABSTRACT

Dispersion characteristics in the Western Mediterranean are analyzed using data from Coastal Ocean Dynamics Experiment (CODE) and Surface Velocity Program (SVP) surface drifters deployed in the period 1986–2017. Results are presented in terms of absolute dispersion A^2 (mean-squared displacement of drifter individuals) and of relative dispersion (D^2; mean square separation distance of drifter pairs). Moreover, the dispersion characteristics are estimated for different initial separation distances (D_0) between particles: smaller, larger, or comparable with the internal Rossby radius of deformation. Results show the presence of a quasiballistic regime for absolute dispersion at small time scales and the nonlocal relative dispersion regime related to the submesoscale activities for scales smaller than the internal Rossby radius. At intermediate times, two anomalous absolute dispersion regimes (elliptic and hyperbolic regimes) related with the flow topology are observed, although the relative dispersion involves the Richardson and shear/ballistic regimes only for D_0 smaller than the Rossby radius. During the subsequent 20–30 days, absolute dispersion shows quasirandom walk regime and relative dispersion follows the diffusive regime for scales larger than 100 km for which pair velocities are uncorrelated.

Keywords: Western Mediterranean, absolute dispersion, relative dispersion, CODE-SVP drifters, anomalous regimes, Richardson regime

1. Introduction

The diagnostic of spread of particles in the ocean can be quantified into two statistics. Firstly, describing how a tracer cloud spreads from its release point as a function of the eddy fluctuations in a turbulent flow field can be studied with one or single particle statistics "absolute dispersion" (Lumpkin and Elipot 2010). Secondly, the spreading about the center of mass of a cloud at small scales involves the two or pair statistics "relative dispersion" (LaCasce 2008; Koszalka et al. 2009; Lumpkin and Elipot 2010). Absolute dispersion

1. Université de Tunis El Manar, Unité de recherche Rayonnement thermique, Faculté des Sciences de Tunis, Tunisie.
2. Corresponding author ***e-mail: maherbouzaiene73@gmail.com***
3. National Institute of Oceanography and Experimental Geophysics, Sgonico (Ts), Italy.
4. Centre for Marine Research and Experimentation, CMRE, La Spezia, Italy.

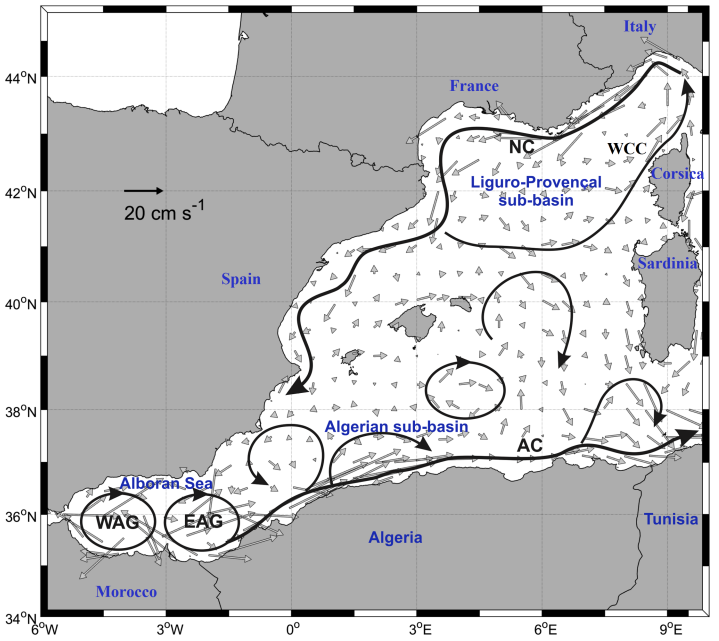

Figure 1. The mean surface circulation and the major circulation features in the westernmost side of the Western Mediterranean (WWM) for the period 1992–2017 based on drifter observations by using the MedSVP_db24 data base organized in bins of 0.5 ° × 0.5 °. The mean currents are shown in gray arrows and the locations of the main circulation features are emphasized in black: Western Algerian Gyre (WAG), the Eastern Algerian gyre (EAG), the Algerian current (AC), the Western Corsican Current (WCC), and the North Current (NC).

quantifies the advection of a cloud of tracer in a turbulent flow (Davis 1991). Moreover, it characterizes the absolute rate of a cloud spreading at large scales (Lumpkin and Elipot 2010). Relative dispersion provides a description of the spreading of fluid particles under chaotic advection and turbulent motions (Schroeder et al. 2011). It is used in many practical applications, such as for understanding and predicting the spreading of pollutants and biological quantities in the ocean (Koszalka et al. 2009; Schroeder et al. 2011). In addition, it gives valuable information about flow structures over many scales of motion (Corrado et al. 2017). An improved understanding of how the eddying ocean mixes both particles and tracers can help quantify the impact of eddies on climate and ecosystems (Sebille et al. 2015).

The westernmost side of the Western Mediterranean (WWM), defined hereafter as the area west of Sardinia and Corsica islands (see Fig. 1), represents an interesting dynamical area characterized by strong coastal currents and mesoscale and basin-scale eddies. The surface circulation in the WWM is relatively complex owing to the presence of coherent vortices that have a great impact on the distribution of water masses and the evolution of

biological quantities. The mean basin-scale circulation is cyclonic (Poulain et al. 2013): the zonal motion is dominant in the Algerian subbasin (AB; Nefzi et al. 2014), whereas the meridional motion characterizes the coast of the Liguro–Provençal subbasin (LPB). In the Alboran Sea the surface currents describe two strong anticyclonic structures (speeds exceeding 30 cm/s) defined as the Western Alboran Gyre (WAG) and the Eastern Alboran Gyre (EAG), respectively (Poulain et al. 2012b; Renault et al. 2012).

Along the Algerian and Tunisian coasts the Algerian Current (AC) moves from west to east, with velocities as large as 30 cm/s (Poulain et al. 2012b) and develop intense eddies (Algerian eddies) with different spatial scales and diameters of about 100–300 km (Testor et al. 2005). Algerian eddies, generated by the instability of the along-slope current (Millot 1999), affect strongly the local ecosystem and induce a crucial variability of marine species (Taupier-Letage et al. 2003). In the LPB the surface currents are involved in a cyclonic circulation reinforced by the wind stress curl (Pinardi et al. 2006; Poulain el al. 2012a), with a strong south-westward boundary current, the Northern Current (NC), characterized by maxima speeds as large as 40–90 cm/s (Poulain el al. 2012a). The NC is affected by instability processes that lead to the generation of submesoscale eddies (Casella et al. 2014). In the eastern part of LPB (west of Corsica), the northward Western Corsican Current (WCC) completes the cyclonic circulation, leads to upwelling of nutrient-rich and colder water, and generates a cyclonic gyre (for details, see Schroeder et al. 2011; Poulain el al. 2012a; Casella et al. 2014).

Nowadays, it is well known that the presence of coherent eddies in the flow induces a discrepancy between the measured or modeled statistical laws and theoretical predictions (Elhmaidi et al. 1993; Nefzi et al. 2014). In this work, we use the database of drifters available in the WWM to analyze the dispersive properties of the upper layer and to investigate the role of surface and subsurface eddies on the dispersion in this region, through the observations of the trajectories of one and two particle statistics computed from drifter data.

One-particle statistics (mean-squared displacement) play a major role in the resolution of the theory of turbulence and understanding the transport of Lagrangian trajectories in the ocean. It is defined by (Poulain and Niiler 1989) as follows:

$$A_i^2(t, t_o) = \left\langle (x_i(t) - x_{0i}(t_0) - < u_i(t - t_o) >)^2 \right\rangle \tag{1}$$

where $x_{0i}(t_0)$ and $x_i(t)$ are respectively vector positions of particles at times t_0 and t, respectively; index i is the i-direction of velocity or position vectors (in case of 2-D turbulence I = 1, 2), $\langle \cdot \rangle = \frac{1}{N} \sum_{k=1}^{N} (\cdot)$ is the Lagrangian average on all individual drifters, N is a number of individual drifters, and $< u_i >$ is the averaged velocity from the global data set. For statistically stationary flows, $A_i(t,t_o)$ depends only on $t-t_0$, and if $t_0 = 0$, characteristic regimes can be distinguished for small, intermediate, and long time scales compared with the Lagrangian decorrelation time scale (Taylor 1921; Elhmaidi et al. 1993).

The so-called Lagrangian decorrelation time scale (T_L) indicates the corresponding time scale at which the drifter still contains information about its past trajectory (Sansón 2015). It is smaller than 5 days in the ocean (Poulain and Niiler 1989).

For homogeneous and stationary field, the absolute diffusivity defined as the derivative of the absolute dispersion in function of time, firstly derived by Taylor (1921), is defined as:

$$k_i(t) = \frac{1}{2}\frac{d}{dt}(A_i{}^2(t)) \tag{2}$$

Many studies have been focused on one-particle statistics in the ocean. They highlighted different regimes presented below:

- the ballistic regime occurs at small times, less than the decorrelation time T_L; the absolute dispersion and the diffusivity grow as t^2 and t, respectively (Taylor 1921; Davis 1983; Poulain and Niiler 1989; Babiano et al. 1985; Elhmaidi et al. 1993).
- The so-called "anomalous" dispersion regimes characterize the strain and vorticity gradients in two-dimensional flows and the dominance of one over the other reflects the presence of hyperbolic and elliptic regions, respectively (Elhmaidi et al. 1993; Provenzale 1999; Castilla et al. 2007). The anomalous regimes take place at intermediate times depending on the dominance of elliptic or hyperbolic regions. $A^2(t)$ shows a t^{α} where α vary between 1 and 2. Numerical studies on neutral floats in two-dimensional flows separated the two-dimensional flow into different regions using the spatial distribution of the Okubo–Weiss parameter ($W = \sigma_s^2 + \sigma_n^2 - w^2$), where $\sigma_s = (\partial_x v + \partial_y u)$, $\sigma_n = (\partial_x u - \partial_y v)$, and $w = (\partial_x v - \partial_y u)$ are the shear strain component, the normal strain component, and the relative vorticity (Okubo et al. 1970; Weiss 1991), respectively. These studies indicated that $\alpha = 5/4$ corresponds to hyperbolic regions in which the deformation dominates the rotation ($W > 0$), whereas $\alpha = 5/3$ corresponds to elliptic regions in which the rotation dominates the deformation ($W < 0$), and finally the background field in which the deformation and the rotation are balanced ($W \approx 0$) (Elhmaidi et al. 1993; Provenzale 1999).
- the random-walk or Brownian regime starts at long time scales where the absolute dispersion grows linearly in time and the diffusivity is constant (Taylor 1921; Davis 1983; Poulain and Niiler 1989; Babiano et al. 1985; Elhmaidi et al. 1993; Sansón 2015).

The two asymptotic regimes (ballistic and Brownian regimes) were observed in numerical simulations of forced and dissipated two-dimensional turbulence (Elhmaidi et al. 1993, Castilla et al. 2007). In real flows, the Brownian regime was detected when the flow is homogenous or the presence of coherent structures in most geophysical flows makes the detection of this regime impossible. The ballistic regime was found in the California (Poulain and Niiler 1989; Sansón 2015) from satellite-tracked drifters, in the subsurface North Atlantic for subsurface floats (LaCasce and Bower 2000), in the Arctic Ocean using data deployed during the SEDNA (Sea Ice Experiment: Dynamic Nature of the Arctic) and

IPY (The International Polar Year)-CFL (Circumpolar Flaw Lead) field campaigns from spring to winter 2008 (Lukovich et al. 2015). The random walk regime was found at sufficiently long times (Taylor 1921; Davis 1983; Poulain and Niiler 1989; Babiano et al. 1985; Elhmaidi et al. 1993; LaCasce and Bower 2000; Sansón 2015, Lukovich et al. 2015).

The anomalous regimes are related to the presence of coherent structures owing to the strong vorticity gradients. These regimes are found numerically during intermediate time scales (Elhmaidi et al. 1993; Castilla et al. 2007). Likewise, LaCasce and Bower (2000) suggested the presence of an intermediate anomalous regime for floats deployed in the North Atlantic at 700-m depth due to the influence of elliptical regions.

The two particle statistics (relative dispersion), which is the measure of the mean square separation distance of particle pairs, is defined as follows (Richardson 1926; Babiano et al. 1990; Ohlmann et al. 2012):

$$D^2(t, D_0) = \left\langle (X_i(t, D_0) - X_j(t, D_0))^2 \right\rangle \tag{3}$$

where $\langle . \rangle = \frac{1}{N_P} \sum_{i \neq j} (.)$ is a Lagrangian average on all pairs, N_P is the number of drifter pairs, indices i and j are for particles, and $X_i(t, D_0)$ and $X_j(t, D_0)$ are the vector positions of the particle positions initially separated by D_0.

In two-dimensional, stationary turbulence the relative diffusivity and the characteristic dispersion time are defined respectively by (Babiano et al. 1990):

$$Y(t, D_0) = \frac{1}{2} \frac{d(D^2(t, D_0))}{dt} \tag{4}$$

$$\tau(t, D_0) = \frac{D^2(t, D_0)}{Y(t, D_0)} \tag{5}$$

The relative diffusivity is related to the mean square relative velocity $\langle \delta v^2(t, D_0) \rangle$ that is used in homogeneous, stationary, and isotropic two-dimensional turbulence to analyze the correlated or uncorrelated pair velocities (Babiano et al. 1990; Koszalka et al. 2009; Ohlmann et al. 2012). The mean square relative velocity is defined by (LaCasce 2008; Ohlmann et al. 2012; Beron-Vera and LaCasce 2016):

$$\begin{aligned} < \delta v^2(t, D_0) > &= < (u_i'(t, D_0) - u_j'(t, D_0))^2 > \\ &= < u_i'^2 > + < u_j'^2 > -2 < u_i' u_j' > \\ &= 4E - 2 < u_i' u_j' > \end{aligned} \tag{6}$$

where u_i' and v_j' are the residual velocities of particles (i.e., $u_i'(t) = u_i(t) - \langle u_i(t) \rangle$) considered in pairs and E is the eddy kinetic energy defined as $E = \frac{1}{2} \left\langle u_i'^2 \right\rangle$. For uncorrelated pair velocities, the mean square relative velocity tends to four times the eddy kinetic energy.

In the last decades several studies have been focused on the relative dispersion in many parts of the World Ocean using in situ measurements. These studies identified four temporal

regimes—depending on the time t, the separation distance between the pairs D_0, and on the forcing injection scale D_I. In two-dimensional turbulence, D_I is the energy injection scale estimated as the internal Rossby radius of deformation. D_I is about 30 km in the ocean (Ollitrault et al. 2005) and varies between 10 and 20 km in the Mediterranean Sea (Schroeder et al. 2011). The above mentioned four regimes are as follows:

- The Lundgren or exponential regime that occurs at small time and separation scale, in which the relative dispersion grows exponentially in time (Lundgren 1981; LaCasce 2010) The dispersion is nonlocal and advected by eddies with scales larger than the separation distance. The relative diffusivity $Y(t, D_0)$ should scale as D^2 in the enstrophy cascade range (Lin 1972) and it increases linearly in time $Y(t, D_0) \propto t$ (LaCasce and Bower 2000) for scale smaller than D_I.
- The Richardson regime that takes place at intermediate times for small initial distances is characterized by pair spreading driven by eddies with the same scale as the separation distance, and the relative dispersion grows as t^3 (Bennett 1984; Babiano et al. 1990). The relative diffusivity $Y(t, D_0)$ and the characteristic dispersion time $\tau(t, D_0)$ should scale respectively as $D^{4/3}$ (Richardson 1926) and $D^{2/3}$ in the inverse energy cascade range (Babiano et al. 1990).
- The Ballistic regime takes place at intermediate times and intermediate initial distances. In this regime, the shear/relative dispersion increases quadratically $D^2(t, D_0) \sim t^2$ (Young et al. 1982; Corrado et al. 2017).
- The Rayleigh or diffusive regime starts at sufficiently long time and for large pair separation. The relative dispersion shows a linear growth in time $D^2(t, D_0) \sim t$ (local regime) and the mean square relative velocity becomes just four times the eddy kinetic energy $\langle \delta v^2(t, D)_0 \rangle \sim 4E$. In this case the pair velocities become uncorrelated and the relative diffusivity becomes constant at large scale and equal to twice the absolute diffusivity (LaCasce and Bower 2000; Ollitrault et al. 2005).

The exponential regime was found in the Gulf of Mexico for the first 2–3 days with $D_0 <$ 1 km and separation distance between 40 and 50 km (LaCasce and Ohlmann 2003), in the Santa Barbara Channel for the first 5 hours of sampling with $5 < D_0 < 10$ m (Ohlmann et al. 2012), in the Gulf of California for the first few days with $D_0 \sim$35 km (Sansón 2015), and in the southwestern Gulf of Mexico for the first 3 days with $D_0 < 2$ km (Sansón et al. 2017) in the whole global ocean and at scale below the Rossby radius (Corrado et al. 2017). In the Mediterranean Sea the relative dispersion increases exponentially with time for the first 6 hours in the Gulf of La Spezia and D_0 of approximately 100 m (Haza et al. 2010), for time scale between 4 and 7 days in the Liguro–Provençal basin with $D_0 < 1$ km and separation distance of 10–20 km (Schroeder et al. 2011), and for the first day in the Adriatic Sea with $D_0 < 1$ km (Poulain et al. 2013).

The Richardson regime was observed in the Nordic Seas for time scale between 2 and 10 days and $D_0 < 2$ km (Koszalka et al. 2009) and in the Gulf Stream for $D_0 < 700$ m and separation distance of 1–3 km (Lumpkin and Elipot 2010). In the Gulf of California for

$D_0 \sim 35$ km and separation distance larger than 30 km, in the Northern Gulf of Mexico for the separation scales below 10 km (Poje et al. 2014), in the southwestern Gulf of Mexico for $D_0 < 2$ km and separation distance between 10 and 150 km (Sansón et al. 2017), and in all subbasins and on scales comparable with the Rossby radius or larger (Corrado et al. 2017).

The Ballistic regime follows the exponential phase in the Santa Barbara Channel for time scales larger than 5 hours (Ohlmann et al. 2012); in the Atlantic northern hemisphere it shows the presence of long-range shear ballistic dispersion due to the action of the Gulf Stream (Corrado et al. 2017) and in the Adriatic Sea for time scale of 2–10 days and separation distance between 10 and 30 km (Poulain et al. 2013).

The diffusive regime was found in the Gulf Stream for separation distance of 300–500 km (Lumpkin and Elipot 2010) and in the Adriatic Sea for time scale larger than 10 days and separation distance larger than 30 km (Poulain et al. 2013).

Several works have studied numerically both absolute and relative dispersion regimes by using conditional averages to compare their behaviors at intermediate time scales. Babiano et al. (1990) have related the presence of the anomalous regimes of the absolute dispersion to the Richardson regime in the relative dispersion. The numerical studies of Castilla et al. (2007) have indicated the hyperbolic anomalous regime of absolute dispersion that is related to the hyperbolic regions surrounding vortices and the presence of Richardson two-particle dispersion. Nevertheless, until today we do not have experimental evidences of anomalous regimes and corresponding relative dispersion at intermediate time scales for a real turbulent flow. In this context, WWM can be seen as a "test basin" in which the large availability of in situ drifter data allows us to carry out absolute and relative dispersion studies.

2. Materials and methods

The Mediterranean Sea drifter data set analyzed for this study is named MedSVP_db24 (Menna et al. 2017; Menna et al. 2018a); it is composed of a total of 424 drifters deployed in the WWM during the period 1986–2017. These drifters are mainly of two types: Coastal Ocean Dynamics Experiment (CODE) drifters, designed to measure the currents in the first meter near the surface layer (Davis 1985; Poulain 1999), and Surface Velocity Program (SVP) drifters, equipped with a holey sock drogue centered at 15-m depth, a sea surface temperature sensor, and a tension sensor that allows checking the presence of the drogue (Sybrandy and Niiler 1991; Lumpkin and Pazos 2007). SVP drifters can lose the drogue during their life (hereafter defined as "undrogued"), therefore the velocities become contaminated by the wind generated slip (Menna et al. 2018b). Undrogued drifters can be identified and separated from drogue-on drifters (defined hereafter as "drogued"), using the SVP drogue detection system and/or the correlation with wind velocities (Menna et al. 2018b). Drifter Argos and GPS positions were tracked by the Argos Data Collection and Location System (DCLS—carried by the NOAA polar-orbiting satellites) or via the Iridium satellite

Table 1. Number of drifter pairs as a function of initial separation distances for drifter types.

	CODE pairs		SVP drogued pairs		All SVP pairs		Any pairs	
D_0 (km)	Originals	Chances	Originals	Chances	Originals	Chances	Originals	Chances
0–1.5	12	42	64	120	79	149	99	213
5–6.5	3	56	35	274	56	396	65	520
10–11.5	2	65	20	329	35	499	54	694
20–21.5	1	90	11	390	19	569	22	834

system. Drifter position time series were first edited from spike and outliers, then linearly interpolated at regular 6-h intervals using the kriging technique (Hansen and Poulain 1996). The interpolated positions were low-pass filtered using a Hamming filter (cut-off period at 36 h) in order to remove high-frequency current components (tidal and inertial currents) and were finally subsampled at 6-h intervals. Velocity components were then estimated from centered finite differences of 6-h subsampled positions (Menna et al. 2012; Poulain et al. 2012b; Poulain et al. 2013). Trajectory pair dispersion is estimated separately for all possible combination occurring for a drifter pair (see Table 1): both drifters are CODE, both drifters are SVP drogued, both drifters are SVP drogued and SVP undrogued, or any of the previous cases (no check of the drifter design). The deployment drifter pairs were identified as those deployed together (original pairs), whereas drifter pairs not launched together were defined as independent chance pairs (Morel and Larcheveque 1974; Er-el and Peskin 1981; LaCasce and Ohlmann 2003). When an independent chance pair is found, our procedure is to fix the pair time and wait 5 days after this time before searching for another independent pair. The numbers of original and chance pairs for each drifter type combination and initial separation distances are summarized in Table 1. The different values of D_0 are selected to compare the initial pair separations with the internal Rossby Radius value (10–20 km) in four cases: in the first, D_0 is very small in comparison to the Rossby Radius and varies in the range of 0–1.5 km. In the second case, D_0 is in the range of 5–6.5 km and is smaller than the Rossby Radius. In the third case, D is comparable to the Rossby Radius and it ranges in 10–11.5 km. The fourth one corresponds to a D_0 larger than the Rossby Radius (D_0 = 20–21.5 km). To examine the absolute dispersion of drifters, we chose the largest number of pairs in function of initial separation distance (Pairs in 20–21.5 km; see the last row of Table 1) and we considered one pair as two drifter individuals released at same time in WWM. Several works have used this technique of drifter individuals or "segments" for the calculation of absolute dispersion (Poulain and Niiler 1989; LaCasce and Bower 2000; Sansón 2015). The number of segments and pairs generally decrease with the time after deployment due to the finite operating life of the drifters; in particular, the CODE pairs number dramatically decrease with time and reach one or two pairs at the day 100 (see insets in Fig. 4). Hence, the statistics were calculated during the first 40 days to get more pairs and segments (see the insets of the Figs. 3 and 4).

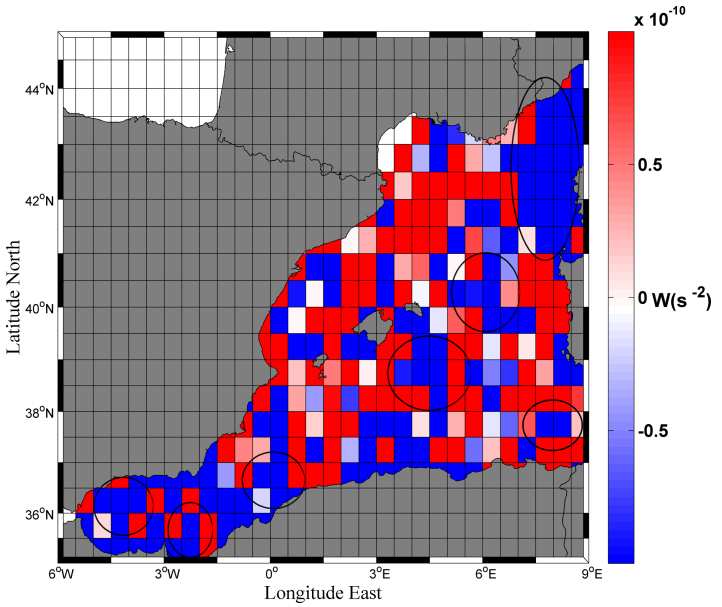

Figure 2. The spatial distribution of the Okubo–Weiss parameter O–W in the westernmost side of the Western Mediterranean (WWM) obtained from drifter observations in 0.5 ° × 0.5 °bins. The O–W is estimated using finite difference of the velocity field. It is coded in color. Blue areas (W < 0) correspond to elliptic regions, red areas (W > 0) correspond to hyperbolic regions, and white indicates the background field (W ∼ 0). The mean subbasin gyres and eddies well known in the WWM are shown with the black ellipses.

3. Results

The surface circulation in the WWM is described in Figure 1 using the MedSVP_db24 data set and adopting the method of Poulain et al. (2013). Our result seems similar to that presented by Poulain et al. (2013) and Pascual et al. (2017), where the mean basin-scale surface circulation is cyclonic with the dominance of the subbasin gyres and eddies observed especially in the AB. A complex surface circulation patterns prevailed in the WWM with different dynamics in each subbasin. The spatial distribution of the Okubo–Weiss parameter O–W in the WWM is displayed in Figure 2 to characterize the flow topology of each subbasin. O–W appears as a set of elliptic regions ($W < 0$, blue), hyperbolic regions ($W > 0, red$), and background field ($W \approx 0, white$). The eastern part of LPB is considered as elliptic domain because of the signature of the cyclonic gyre. On the other hand, the western part of LPB is dominated by hyperbolic regions (Fig. 2). The main eddies of the WWM show an elliptic structure in their core and a hyperbolic structure that surrounds the core (Fig. 2). Our results are comparable with those found in the WWM (Font et al. 2004; Garcia-Olivares et al. 2007; D'Ovidio et al. 2008).

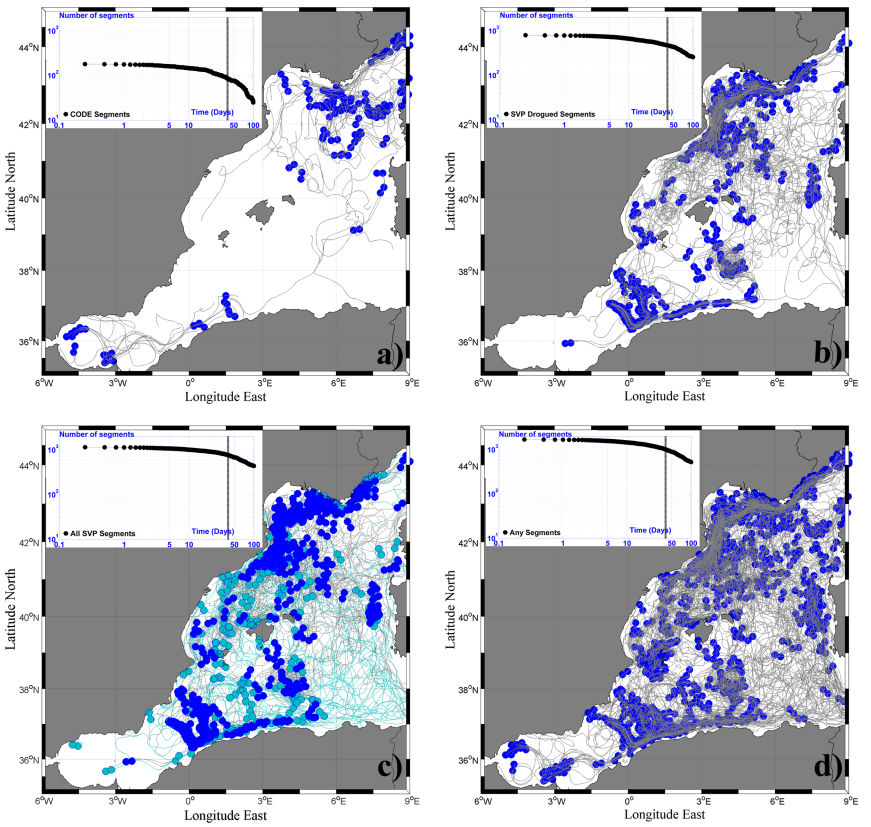

Figure 3. Initial positions of the Coastal Ocean Dynamics Experiment (CODE) (a) Surface Velocity Program (SVP) drogued (b), all SVP (c) (SVP drogued + SVP undrogued) and any segments (d). Initial positions of segments (blue dots). The drifter trajectories during the 100 days are shown in gray color, an exception for SVP undrogued initial positions and trajectories are shown in cyan dots and cyan lines, respectively. In the inset we show the number of segments in function of time. The vertical black lines indicate the days 40 where after this day the number of segments is decreased dramatically in function of time.

The absolute dispersion is calculated for zonal and meridional directions of the WWM in function of drifter types in five cases: CODE, SVP drogued, SVP undrogued, all SVP (putting together both drogued-undrogued), and any segments (Fig. 5). The absolute dispersion is nearly ballistic in both directions in any cases during the first 2 days. From 2 to 6 days, approximately, $A^2(t)$ shows the elliptic regime for the CODE drifters, especially in the zonal direction (Fig. 5a). For the other drifter types, this regime is less pronounced and absolute dispersion follows the 5/4 power law after the sixth day, especially for the meridional direction (hyperbolic regime). For time scales larger than the twentieth days, the drifters lose memory of their initial velocity and a nearly random walk regime takes place

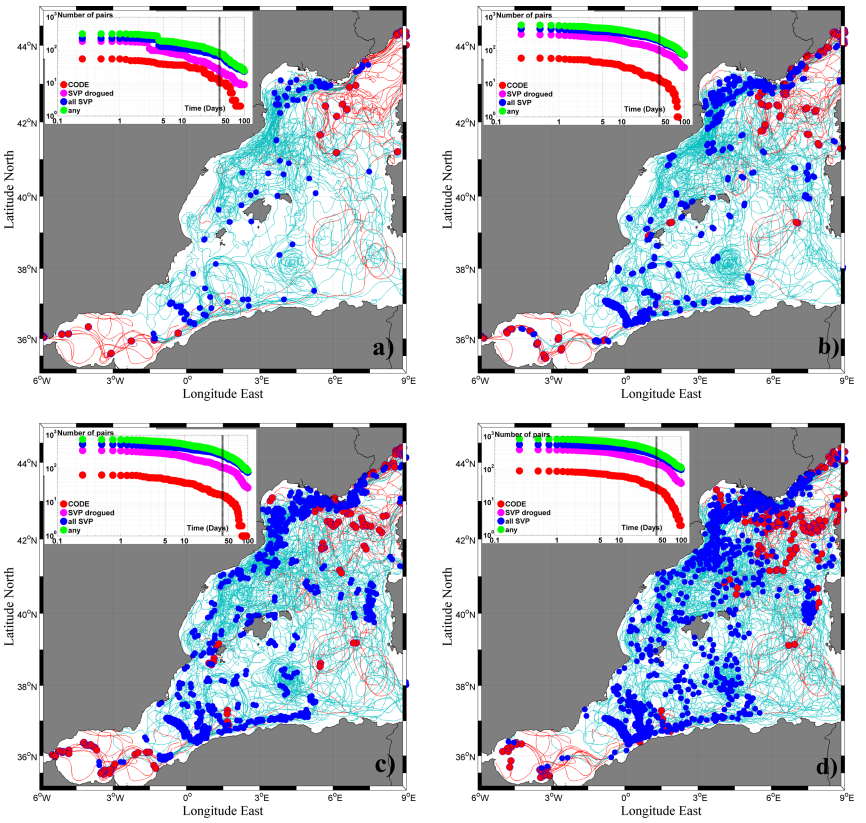

Figure 4. Initial positions of the Coastal Ocean Dynamics Experiment (CODE) and Surface Velocity Program (SVP) pairs (original and chance pairs) with initial separation distances in 0–1.5 km (a), in 5–6.5 km (b), in 10–11.5 km (c), and in 20–21.5 km (d). Initial positions of CODE pairs (red dots), SVP pairs (blue dots), and their trajectories are shown in red and cyan colors, respectively during the 100 days. In the inset we show the number of pair distances in function of time. The vertical black lines show the days 40.

in both directions for the different cases. The zonal component is greater than the meridional component and the dispersion is anisotropic. The large zonal dispersion originates in the presence of the zonal energetic currents (the AC and NC). The Absolute diffusivity shows the two nearly asymptotic regimes (ballistic regime and the random walk regime), and the diffusivity reached a constant value $\sim$400 km^2.days^{-1} (Fig. 6).

The absolute dispersion statistics (Fig. 5) reveal two anomalous regimes: elliptic (5/3) for CODE drifters from 2 to 6 days and the hyperbolic (5/4) for the other drifter types after the day 6, approximately, in the WWM. In order to check the drifter distributions during these anomalous regimes, we superimposed the spatial distribution of the Okubo–Weiss parameter O–W in the WWM to the drifter trajectories during the first twenty days and their positions

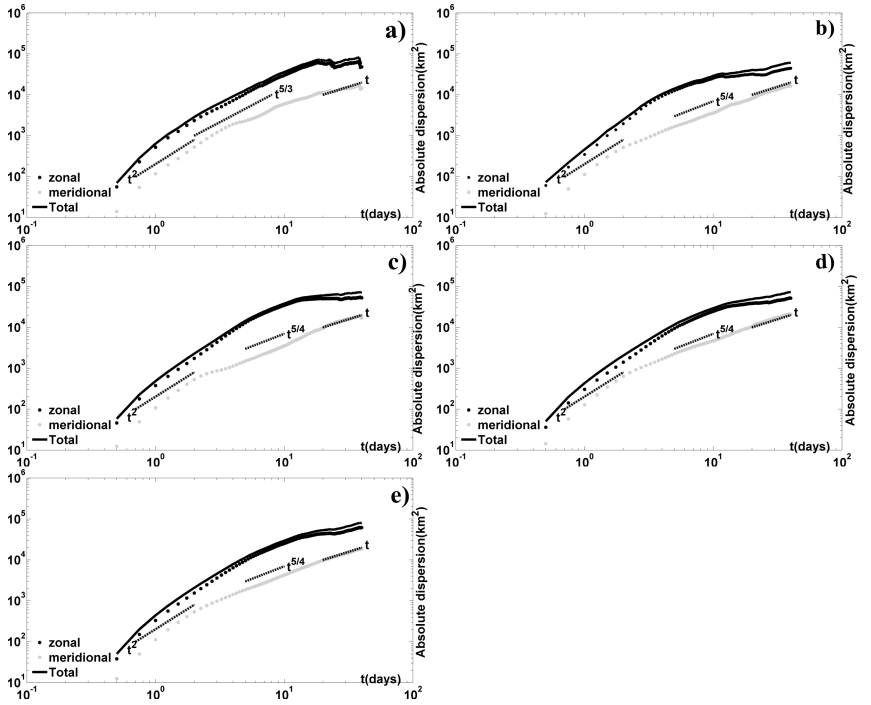

Figure 5. Absolute dispersion of the Coastal Ocean Dynamics Experiment (CODE) (a) Surface Velocity Program (SVP) drogued (b), SVP undrogued (c), all SVP (d), and any segments (e) in a log–log plot in function of time during the first 40 days.

at the sixth day for CODE, SVP drogued, all SVP (SVP drogued and undrogued), and any segments. The drifter number per geographical bins (elliptic, hyperbolic, background field, and out domain) is displayed in the insets of Figure 7.

Results shows that 69% of CODE drifters are mainly located in elliptic bins, especially in the eastern part of the LPB (inside the cyclonic gyre), and in the Alboran basin (Fig. 7a). In agreement to the results of the absolute dispersion (Fig. 5a), these areas can be defined as elliptic regions in which the rotation is more relevant than the strain. Numerous SVP drogued (64%) and undrogued (60%) are located in hyperbolic bins, especially in the western part of the LPB or in the region of the Algerian eddies (see insets of Fig. 7b and c). These results confirm the occurrence of the hyperbolic regime as detected by the absolute dispersion statistics (Fig. 5b and c). When we consider all the drifters together (Fig. 7d), the majority of positions (53%) are located in hyperbolic regions, and only 40% of positions are located in elliptic bins (see insets of Fig. 7d). In this condition, the absolute dispersion (Fig. 5d) emphasizes the presence of the hyperbolic regime that is dominant with respect to the elliptic regime.

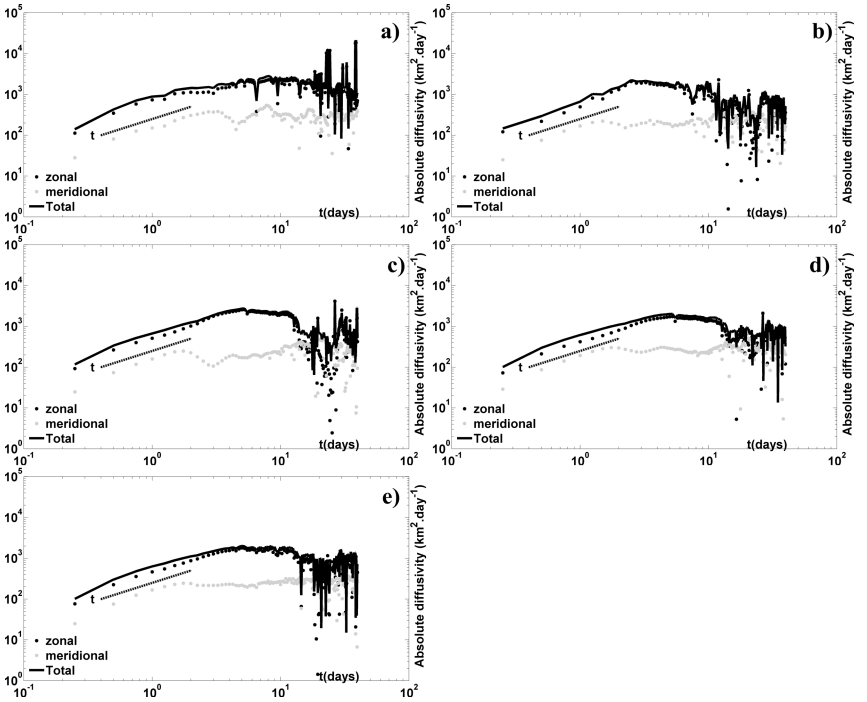

Figure 6. Absolute diffusivity of the Coastal Ocean Dynamics Experiment (CODE) (a) Surface Velocity Program (SVP) drogued (b), SVP undrogued (c), all SVP (d), and any segment (e) drifters in a log–log plot in function of time during the first 40 days.

The relative dispersion was estimated for different drifter types. As the relative dispersion regimes depend on initial separation distances D_0 and on the internal Rossby radius of deformation D_I (Babiano et al. 1990), we considered four cases of D_0 ($D_0 < D_I$, $D_0 \approx D_I$ and $D_0 > D_I$). As for the absolute dispersion, the relative dispersion is estimated averaging the longitudinal and meridional components of the flow.

The relative dispersion is calculated from Eq. 3 and displayed in Figure 8 for different initial separation distances. The temporal evolution of the relative dispersion for the first 3 days after deployment shows an exponential growth for all initial separation distances D_0 and evolves as $e^{\alpha t}$, where α is the growth rate, indicated in Fig. 8a–d). The duration of the exponential growth increases with the increase of initial separation distance: for example, it is about 1 day for the smallest D_0 and reaches 2.5 days for the largest value of D_0. Figure 8e–h shows temporal evolution of D^2 for $1 < t < 40$ days. The Richardson law, t^3, takes place after the exponential growth. This law is well observed for the smallest value of D_0 ($<$1.5 km; Fig. 8e) and for time ranging from 1 to 3 days.

The dispersion is ballistic between 3 and 20 days for $0 < D_0 < 1.5$ km and $5 < D_0 < 6.5$ km (see Fig. 8e and f). The relative dispersion grows as t^{α}, with $1 < \alpha < 2$, between 3 and

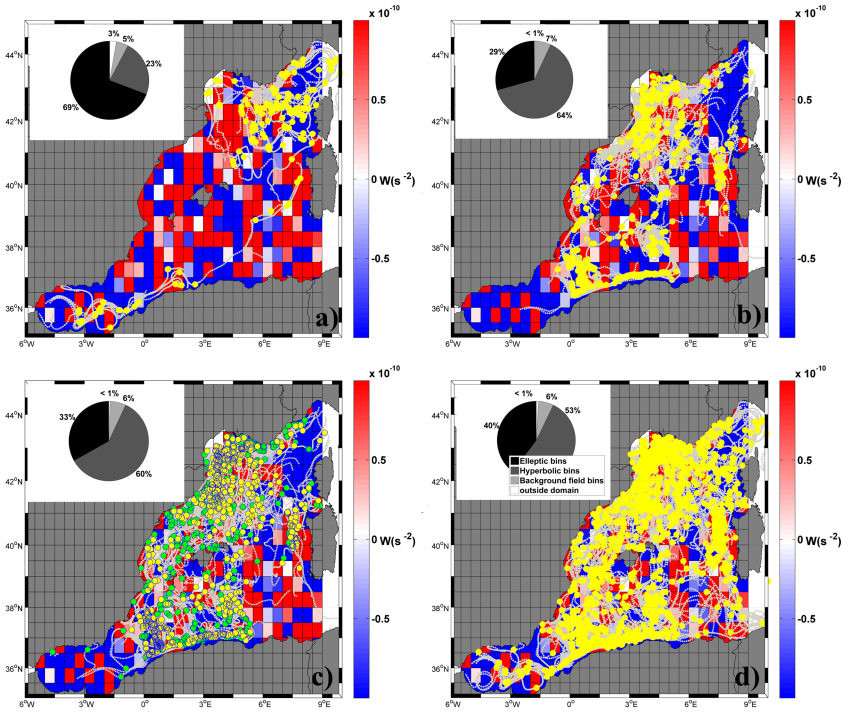

Figure 7. The spatial distribution of the Okubo–Weiss parameter O–W in the westernmost side of the Western Mediterranean (WWM) superposed with the drifter trajectories during the first 20 days and their positions at the sixth day for Coastal Ocean Dynamics Experiment (CODE) (a), Surface Velocity Program (SVP) drogued (b), all SVP (SVP drogued and undrogued) (c) and any segments (d). The drifter positions are shown in yellow dots and the SVP undrogued (green dots) and the drifter trajectories during the 20 days are shown in gray color. In the inset we show the number records of drifters at the sixth day per geographical bins (elliptic, hyperbolic, background field, and out domain).

20 days when $10 < D_0 < 11.5$ km and $20 < D_0 < 21.5$ km (see Fig. 8g and h). For long time scales (more than 20 days), a linear growth of relative dispersion for all initial pair separations is observed (Fig. 8e–h).

The temporal evolution of $\langle \delta v^2(t, D_0) \rangle$ and four time eddy kinetic energy, 4E, was used to describe the behavior of pairs and to estimate the decorrelation time scales of pair velocities (Fig. 9a–d). In the first 10–20 days (depending on the initial separation distance), the 4E is larger than $\langle \delta v^2(t, D_0) \rangle$, because drifters were generally deployed in energetic features like fronts (where the majority of drifter pairs are located in the strong boundary currents along the Liguro–Provençal–Catalan and Algerian coasts; see Fig. 4). After the first 20–30 days, 4E and $\langle \delta v^2(t, D_0) \rangle$ reach approximately the same value, pointing out that the pair velocities are uncorrelated ($2\langle u_i' u_j' \rangle = 0$).

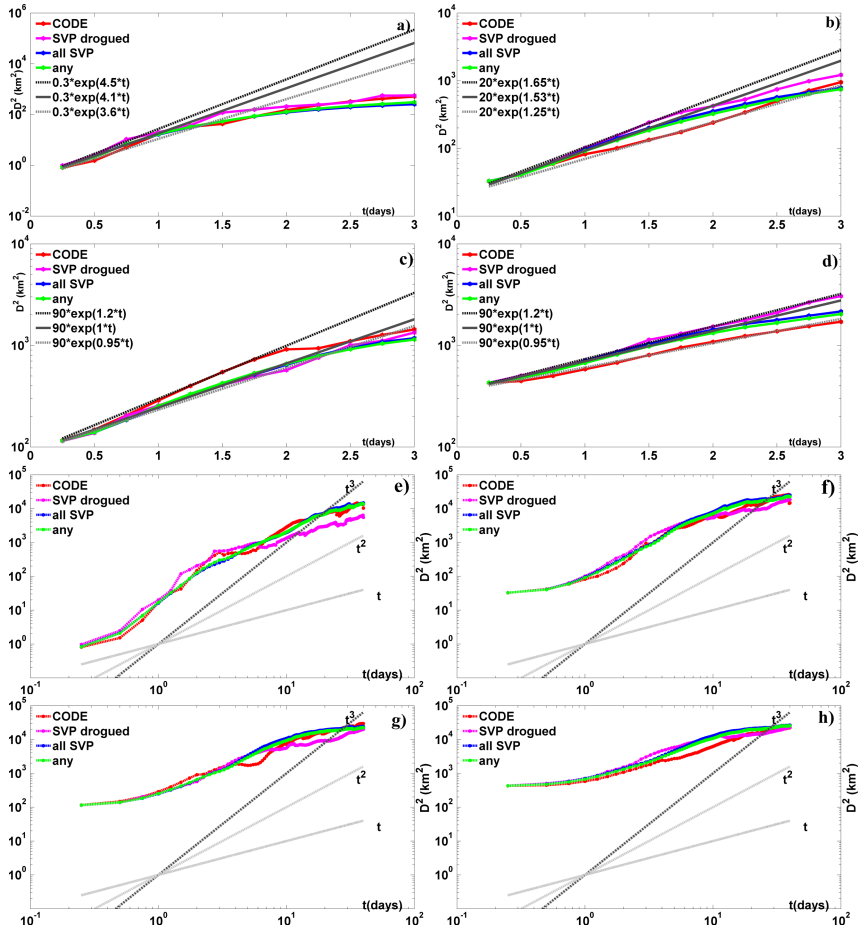

Figure 8. Relative dispersion in a log-linear plot during the first three days of the Coastal Ocean Dynamics Experiment (CODE), Surface Velocity Program (SVP) drogued, all SVP, and any pairs with initial separation distances in 0–1.5 km (a), in 5–6.5 km (b), in 10–11.5 km (c), and in 20–21.5 km (d). Straight lines represent experimental fits. Relative dispersion in a log–log plot versus time after deployment of the Coastal Ocean Dynamics Experiment (CODE), SVP drogued, all SVP, and any pairs with initial separation distances in 0–1.5 km (e), in 5–6.5 km (f), in 10–11.5 km (g), and in 20–21.5 km (h).

During the first three days, we show the temporal evolution of the relative diffusivity reduced by the time t (Fig. 10a–d). Quasilinear increases are observed during the first one day for SVP drogued pairs and extending to the second day for all SVP and any drifter pairs for the $5 < D_0 < 6.5$ km (Fig. 10b). Also, quasilinear increases are detected during the first one day for all SVP and any drifter pairs and extending to the second day for the CODE

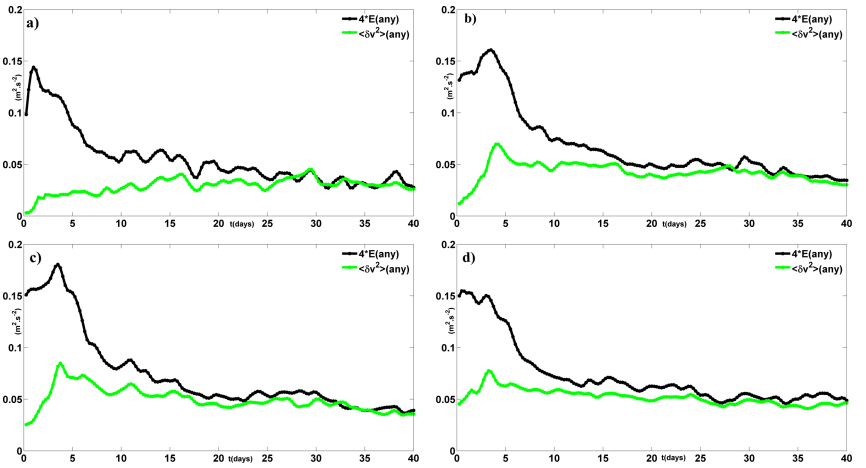

Figure 9. Mean square relative velocity $\langle \delta v^2 \rangle$ and four time eddy kinetic energy 4E of the any pairs with initial separation distances in 0–1.5 km (a), in 5–6.5 km (b), in 10–11.5 km (c), and in 20–21.5 km (d).

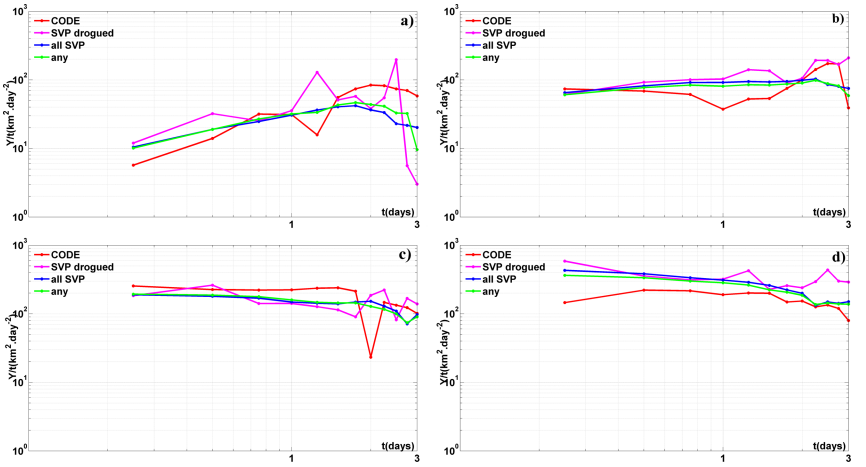

Figure 10. Relative diffusivity divided by the time t in a log–log plot in function of time during the three first days of the Coastal Ocean Dynamics Experiment (CODE), Surface Velocity Program (SVP) drogued, all SVP, and any pairs with initial separation distances in 0–1.5 km (a), in 5–6.5 km (b), in 10–11.5 km (c), and in 20–21.5 km (d).

pairs for $10 < D_0 < 11.5$ km (Fig. 10c). For the other cases of D_0, the quasilinear growth is not detected (Fig. 10a and d).

The relative diffusivity in function of separation distance (Fig. 11a–d) shows a clear exponential growth for CODE pairs for scales smaller than 20 km when the initial separation

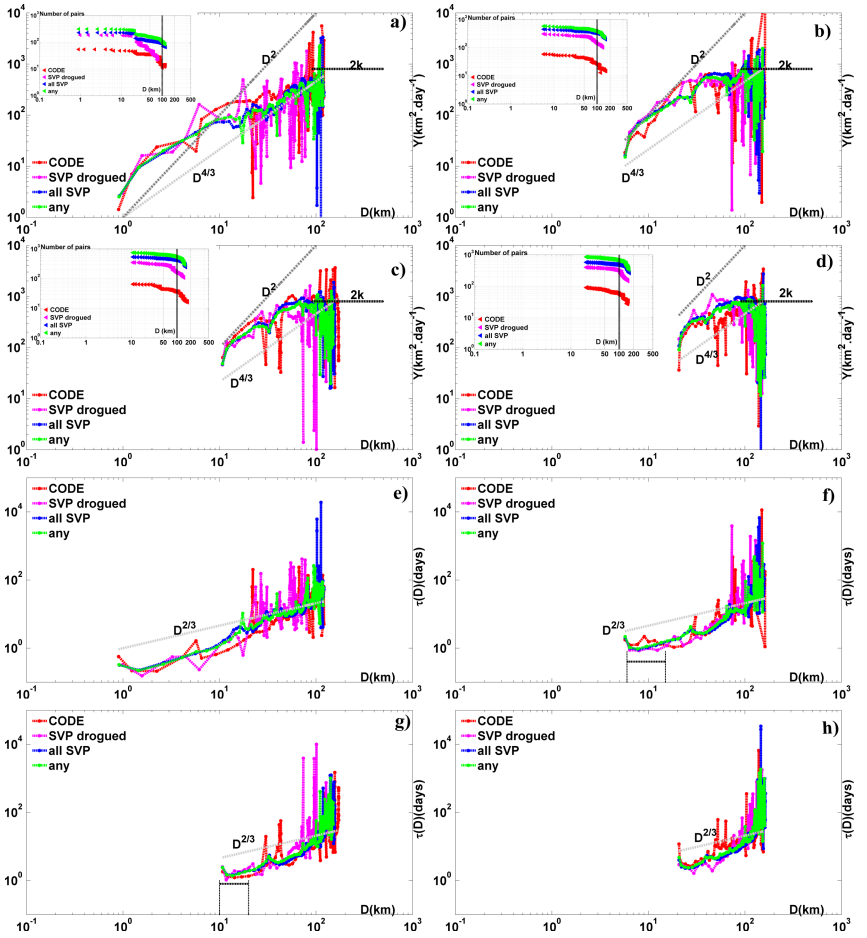

Figure 11. Relative diffusivities in a log–log plot in function of separation distance of the Coastal Ocean Dynamics Experiment (CODE), Surface Velocity Program (SVP) drogued, all SVP, and any pairs with initial separation distances in 0–1.5 km (a), in 5–6.5 km (b), in 10–11.5 km (c), and in 20–21.5 km (d). Characteristic dispersion times $\tau(t, D_0)$ of the CODE, SVP drogued, all SVP, and any pairs with initial separation distances in 0–1.5 km (e), in 5–6.5 km (f), in 10–11.5 km (g), and in 20–21.5 km (h) in a log–log plot in function of separation distance. In the inset we show the number of pair distances in function of separation distances; more than 10 pairs are observed for scales about 100 km (see the vertical black line).

distance is 10–11.5 km; this exponential growth is less pronounced for the other pair types due to the relative quickly increase of the diffusivity (Fig. 11c). Also, the exponential growth is observed for the SVP drogued, all SVP, and any pairs for $5 < D_0 < 6.5$ km, whereas it is not clear for the CODE pairs (Fig. 11b). A point differs: the exponential growth is not observed for the drifter pairs with an initial distance in 20–21.5 km and the diffusivity

tends to reach the diffusive regime due to the initial pair separations are large to the energy containing eddies. For the smallest value of D_0, the exponential phase is less pronounced at small scales and the diffusivity shows the Richardson law for all drifter pairs: It grows approximately as distance to the 4/3 power for the scale ranging from 2 to 10 km (Fig. 11a). At large scales (100 km or more), relative diffusivities are constants and approximately comparable with twice absolute diffusivities for all the values of D_0 because pair velocities are uncorrelated.

A common point is that when the exponential regime occurs in term of diffusivity, the characteristic dispersion time defined in Eq. 5 will be also constant in function of separation distance. It was so in all present four cases presented in previous paragraph and the relative characteristic dispersion time is approximately constant for $D < 20$ km (see Fig. 11f and g). Further, the characteristic dispersion time as a function of initial separation distances of drifter pairs shows a power law $D^{2/3}$ for scale ranging from 2 to 10 km for all pairs with initial distance in 0–1.5 km (Fig. 11e). This result confirms the existence of the Richardson regime in the inverse energy cascade range. For the other initial separation distances, the Richardson law is less pronounced and it ranges, for example, from scale between 20–30 km for $5 < D_0 < 6.5$ km.

In order to ensure robust statistics in the diffusive regime, where the pairs decreased dramatically in function of distance (see insets in Fig. 11), we do not display results when there are less than 10 pairs of drifters (Haza et al. 2014).

4. Discussion

In the present work, we have studied Lagrangian dispersion characteristics of CODE and SVP drifters deployed in the WWM. We mainly focus on the first 40 days and on space scale ranging from 0–1.5 km to the mesoscale (20–21.5 km). Dispersion statistics are estimated both separately for CODE, SVP drogued, and all SVP pairs and also by putting together all of the different drifter designs.

Results are presented in terms of A^2 (mean-squared displacement of drifter individuals) and D^2 (mean square separation distance of drifter pairs).

The absolute dispersion A^2 shows a nearly ballistic regime during the first 2 days and a nearly random walk regime, approximately, for time scales larger than 20 days in function of drifter types for any cases. In our measurements, the absolute dispersion behaviors are not coinciding with the exact theoretical ballistic behavior (quadratic initial dispersion) and the random walk behavior (linear dispersion) for homogeneous and isotropic 2 D turbulent flow. The difference comes from the nonuniform nature of our data set and the different characteristics of the basin; drifters are located in different regions such as in the Liguro–Provençal and along the Algerian coasts. Hence, the dispersion is limited by the north and the south boundaries. The anisotropic character of surface western Mediterranean flow is observed in the largest value of the zonal dispersion, which is due to the presence of zonal gyres or eddies trapping drifters during their travels for few days or weeks. Both anomalous regimes testify the presence of elliptic and hyperbolic regions related to the

high vorticity and high strain regions, respectively, due to the influence of coherent vortices and currents. The elliptic regime ($t^{5/3}$) appears as signature of elliptic regions from 2 to 6 days, only observed for the CODE drifters. The presence of hyperbolic regions induced the hyperbolic regime ($t^{5/4}$) after the sixth day for the SVP drogued, SVP undrogued, all SVP, and any segments. The anomalous two regimes are anisotropic due to the submesoscale and mesoscale features of WWM.

The temporal evolution of D^2 shows an exponential growth in the first 1–2.5 days for all the initial separation distances, on scale below or comparable with the Rossby radius of deformation (Fig. 9a–d). However, this result does not necessarily imply an exponential nonlocal dispersion, as suggested by Sansón et al. (2017) and LaCasce et al. (2010), if the other statistics (the relative diffusivity and characteristic dispersion time) taken into account don't confirm this status: the nonlocal regimes confirmed by relative diffusivity and the relative characteristic dispersion time statistics for the CODE pairs for D_0 of 10–11.5 km and SVP drogued, all SVP, and any pairs for D_0 of 5–6.5 km. These results can be clearly related to the geographical location of the pairs that are mainly located in the Alboran and Ligurian Seas and involved in the local circulation features. The nonlocal dispersion regime is more pronounced for the CODE pairs for D_0 of 10–11.5 km in comparison with the CODE pairs with initial distance in 5–6.5 km, possibly due to the geographic distribution of the CODE pairs that are slightly concentrated in the Alboran Sea for the D_0 of 10–11.5 km (see Fig. 4b and c). Curiously, the exponential regime is not observed for the smallest value of D_0 for all drifter types. A possible explanation is a rapid growth of pair separations does not allow observing the nonlocal regime and the relative dispersion would enter directly into the Richardson regime. In addition, the 6-hourly resolution of our data set can contaminate the presence of the nonlocal regime for small scales. The Richardson regime (t^3) is clear in the first 1–3 days for D_0 smaller than 1.5 km (Fig. 8e), on scale comparable with the Rossby radius; this regime is also confirmed by the relative diffusivity $D^{4/3}$ and the characteristics dispersion time ($D^{2/3}$) statistics for range scale of 2–10 km (Fig. 11a and e).

The shear/ballistic regime (t^2), due to the action of boundary currents (Algerian and Liguro–Provençal–Catalan currents), is observed for D_0 of 0–1.5 km and 5–6.5 km and between 3 and 20 days (Fig. 8e and f). For larger separation distances, the relative dispersion grows as t^{α}, with $1 < \alpha < 2$, between 3 and 20 days, showing a behavior in the middle between the ballistic and diffusive regimes (Fig. 8g and h).

The diffusive regime (t) starts after 20–30 days for all D_0 and for scales larger than 100 km; it is characterized by pair separation larger than the size of the dominant eddies. In this situation the relative diffusivity is approximately constant and all pair relative velocities are uncorrelated.

5. Conclusion

In this paper we indicate the possible occurrence of anomalous absolute dispersion regimes, the Richardson and shear/ballistic relative dispersion regimes at intermediate time

scales for real turbulent flows using a large data set (1986–2017). Elliptic ($t^{5/3}$) and hyperbolic ($t^{5/4}$) regimes are related to the flow topology of the WWM, as reported in Elhmaidi et al. (1993) and Castilla et al. (2007), respectively. The ($t^{5/3}$) regime is related to the particle dispersion in the core of coherent structures where the rotation is more relevant than the strain (elliptic regions). The $t^{5/4}$ regime appears as the signature of hyperbolic energetic domains surrounding coherent vortices where the Okubo–Weiss parameter is positive. In hyperbolic regions where the shear is important, the shear/ballistic regime for the relative dispersion takes place. The Richardson regime is observed for small initial separation distance $D_0 < 1.5$ km.

This study for the first time relates the anomalous absolute dispersion regimes at intermediate time scales with the flow topology in WWM, looking at the relative dispersion regimes occurring at these middle times in a real turbulent flow. The results of this work represent a first attempt to characterize an entire Mediterranean subbasin in terms of absolute and relative dispersion. Previous studies realized in the Mediterranean Sea have analyzed very local aspects related to limited geographical regions (i.e., Ligurian Sea in Schroeder et al. 2011 or the Adriatic Sea in Poulain et al. 2013). We aim to extend this method to the other Mediterranean subbasins in order to compare the different dispersion regimes and define the parameters common to all ocean subbasins.

Acknowledgments. We thank all the people who deployed drifters in the Western Mediterranean and kindly shared their data. This work was supported by the Ministry of Higher Education, Scientific Research and Technology of Information and Communication in the frame work of the Tuniso–Italian collaboration between; the Université de Tunis El Manar, Faculté des Sciences de Tunis, Unité du Rayonnement Thermique, Tunisie and National Institute of Oceanography and Experimental Geophysics, Sgonico (Ts), Italy. We are grateful to Antonio Bussani and Thomas Miraglio for their technical advice about drifters.

REFERENCES

Babiano, A., C. Basdevant, and M. Larchevêque. 1985. Fonction de structure et spectre lagrangiens d'un écoulement turbulent bidimensionnel, CR. Acad. Sei. Paris, *300*, 195–198.

Babiano, A., C. Basdevant, P. LeRoy, and R. Sadourny. 1990. Relative dispersion in two-dimensional turbulence, J. Fluid Mech., *214*, 535–557. doi: 10.1017/S0022112090000258

Bennett, A.F. 1984. Relative dispersion: local and nonlocal dynamics, J. Atmos. Sci., *41*, 1881–1886. doi: 10.1175/. 1520-0469(1984)041,1881:RDLAND.2.0.CO

Beron-Vera, F. J., and J. H. LaCasce. 2016. Statistics of simulated and observed pair separations in the Gulf of Mexico, J. Phys. Oceanogr., *46*, 2183–2199. doi: 10.1175/JPO-D-15-0127.1

Casella, E., P. Tepsichi, X. Couvelard, R.M.A. Caldeira, and K. Schroeder. 2014. Ecosystem dynamics in the Liguro-Provençal Basin: the role of eddies in the biological production, Mediterr. Mar. Sci., *15*, 274–286. doi: 10.12681/mms.520

Castilla, R., J. M. Redondo, P. J. Gámez-Montero, and A. Babiano. 2007. Particle dispersion processes in two-dimensional turbulence: a comparison with 2-D kinematic simulation, Nonlinear Process. Geophys., *14*, 139–151. doi: 10.5194/npg-14-139-2007

Corrado, R., G. Lacorata, L. Palatella, R. Santoleri, and E. Zambianchi. 2017. General characteristics of relative dispersion in the ocean, Sci. Rep., *7*, 46291. doi: 10.1016/j.rse.2018.11.013

Davis, R. E. 1983. Oceanic property transport, Lagrangian particle statistics, and their prediction, J. Mar. Res. *41*, 163–194. doi: 10.1357/002224083788223018

Davis, R. E. 1985. Drifter observation of coastal currents during CODE: the method and descriptive view, J. Geophys. Res. Oceans, *90*, 4741–4755. doi: 10.1029/JC090iC03p04741

Davis, R. E. 1991. Observing the general circulation with floats, Deep Sea Res. A, *38*(Suppl), S531–S571. doi: 10.1016/S0198-0149(12)80023-9

D'Ovidio, F., J. Isern-Fontanet, J. Lopez, E. Hernandez-Garcia, and E. Garcia-Ladona. 2008. Comparison between Eulerian diagnostics and finite-size Lyapunov exponents computed from altimetry in the Algerian basin, Deep Sea Res. Part I Oceanogr. Res. Pap., *56*, 15–31. doi: 10.1016/j.dsr.2008.07.014

Elhmaidi, D., A. Provenzale, and A. Babiano. 1993. Elementary topology of the two-dimensional turbulence from a Lagrangian viewpoint and single particle dispersion, J. Fluid Mech., *257*, 533–558. doi: 10.1017/S0022112093003192

Er-el, J., and R. Peskin. 1981. Relative diffusion of constant-level balloons in the Southern hemisphere, J. Atmos. Sci., *38*, 2264–2274. doi: 10.1017/S0022112093003192

Font, J., J. Isern-Fontanet, and J. D. J. Salas. 2004. Tracking a big anticyclonic eddy in the western Mediterranean Sea, Sci. Mar., *68*, 331–342. doi: 10.1029/1999JC000117

Griffa, A., A. D. Kirwan, Jr., A. J. Mariano, T. M. Özgökmen, and H. T. Rossby. 2007. Lagrangian Analysis and Prediction of Coastal and Ocean Dynamics. Cambridge: Cambridge University Press, 487 pp.

Hansen, D. V., and P.-M. Poulain. 1996. Quality control and interpolations of WOCE-TOGA drifter data, J. Atmos. Ocean. Technol., *13*, 900–909. doi: 10.1175/1520-0426(1996)013<0900:QCAIOW>2.0.CO;2

Haza, A. C., T. M. Özgökmen, A. Griffa, A. Molcard, P.-M. Poulain, and G. Peggion. 2010. Transport properties in small-scale coastal flows: relative dispersion from VHF radar measurements in the Gulf of La Spezia, J. Ocean. Dyn., *60*, 861–882. doi: 10.1007/s10236-010-0301-7

Haza, A. C., T. M. Özgökmen, A. Griffa, A. C. Poje, and M.-P. Lelong. 2014. How does drifter position uncertainty affect ocean dispersion estimates? J. Atmos. Ocean Technol., *31*, 2809–2828. doi: 10.1175/JTECH-D-14-00107.1

Koszalka, I., J. H. LaCasce, and K. A. Orvik. 2009. Relative dispersion in the Nordic Seas, J. Mar. Res., *67*, 411–433. doi: 10.1357/002224009790741102

LaCasce, J. H. 2008. Statistics from Lagrangian observations, Progr. Oceanogr., *77*, 1–29. doi: 10.1016/j.pocean.2008.02.002

LaCasce, J. H. 2010. Relative displacement probability distribution functions from balloons and drifters, J. Mar. Res., *68*, 433–457. doi: 10.1357/002224010794657155

LaCasce, J. H., and A. Bower. 2000. Relative dispersion in the subsurface North Atlantic, J. Mar. Res., *58*, 863–894. doi: 10.1357/002224000763485737

LaCasce, J. H., and C. Ohlmann. 2003. Relative dispersion at the surface of the Gulf of Mexico, J. Mar. Res., *61*, 285–312. doi: 10.1357/002224003322201205

Lin, J.-T. 1972. Relative dispersion in the enstrophy-cascading inertial range of homogeneous two-dimensional turbulence, J. Atmos. Sci., 29, 394–395. doi: 10.1175/1520-0469(1972)029,0394:RDITEC.2.0.CO;2

Lumpkin, R., and S. Elipot. 2010. Surface drifter pair spreading in the North Atlantic, J. Geophys. Res., *115*, C12017. doi: 10.1029/2010JC006338

Lumpkin, R., and M. Pazos. 2007. Measuring surface currents with SVP drifters: the instrument, its data and some results, *in* Lagrangian Analysis and Prediction of Coastal and Ocean Dynamics. A. Mariano, T. Rossby, and D. Kirwan, eds. Cambridge: Cambridge University Press, 39–67.

Lukovich, J. V., J. K. Hutchings, and D. G. Barber. 2015. On sea-ice dynamical regimes in the Arctic Ocean, J. Ann. Glaciol., 56, 323–331. doi: 10.3189/2015AoG69A606

Lundgren, T. S. 1981. Turbulent pair dispersion and scalar diffusion, J. Fluid Mech., *111*, 27–57. doi: 10.1017/S0022112081002280

Menna, M., R. Gerin, A. Bussani, and P.-M. Poulain. 2017. The OGS Mediterranean drifter database: 1986-2016, technical report 2017/92 Sez, Trieste, Italy: OGS 2017/92 OCE 28 MAOS. 34 pp.

Menna, M., R. Gerin, A. Bussani, and P.-M. Poulain. 2018a. Surface currents and temperature data, db_med24_nc_1986_2016_kri05–db_med24_nc_1986_2016_kri6hF. doi: 10.6092/7a8499bc-c5ee-472c-b8b5-03523d1e73e9

Menna, M., P-M. Poulain, A. Bussani, and R. Gerin. 2018b. Detecting the drogue presence of SVP drifters from wind slippage in the Mediterranean Sea. Measurement, *125*, 447–453. doi: 10.1016/j.measurement.2018.05.022

Menna, M., P.-M. Poulain, G. Zodiatis, and I. Gertman. 2012. On the surface circulation of the Levantine sub-basin derived from Lagrangian drifters and satellite altimetry data, Deep Sea Res. Part I Oceanogr. Res. Pap., *65*, 46–58. doi: 10.1016/j.dsr.2012.02.008. doi: 10.1016/j.dsr.2012.02.008

Millot, C.1999. Circulation in the Western Mediterranean sea, J. Mar. Syst., *20*, 423–442. doi: 10.1016/S0924-7963(98)00078-5

Morel, P., and M. Larcheveque. 1974. Relative dispersion of constant level balloons in the 200 mb general circulation, J. Atmos. Sci., *31*, 2189–2196. doi: 10.1175/1520-0469(1974)031<2189:RDOCBI>2.0.CO;2

Nefzi, H., D. Elhmaidi, and X. Carton. 2014. Turbulent dispersion properties from a model simulation of the western Mediterranean Sea, J. Ocean Sci., *10*, 167–175. doi: 10.5194/os-10-167-2014

Ohlmann, J. C., J. H. LaCasce, L. Washburn, A. J. Mariani, and B. Emery. 2012. Relative dispersion observations and trajectory modeling in the Santa Barbara, J. Geophys. Res., *117*, C05040. doi: 10.1029/2011JC007810

Okubo, A. 1970. Horizontal dispersion of floating particles in the vicinity of velocity singularities such as convergence, J. Deep-sea Res. Oceanogr. Abstr., *17*, 445–454. doi: 10.1016/0011-7471(70)90059-8

Ollitrault, M., C. Gabillet, and A. Colin de Verdiere. 2005. Open ocean regimes of relative dispersion, J. Fluid Mech., *533*, 381–407. doi: 10.1017/S0022112005004556

Pascual, A., S. Ruiz, A. Olita, C. Troupin, M. Claret, B. Mourre, B. Casas, et al. 2017. A Multiplatform Experiment to Unravel Meso- and Submesoscale Processes in an Intense Front (AlborEx), Front. Mar. Sci. 4:39. doi: 10.3389/fmars.2017.00039

Pinardi, N., M. Zavatarelli, E. Arneri, A. Crise, and M. Ravaioli. 2006. The physical, sedimentary and ecological structure and vari-ability of shelf areas in the Mediterranean Sea, *in* The Sea: Ideas and Observations on Progress in the Study of the Seas, vol. 14, The Coasts of Africa, Europe, Middle East, Oceania and Polar Regions. A. R. Robinson and K. H. Brink, eds. Cambridge, MA: Harvard University Press, 1245–1330.

Poje, A. C., T. M. Özgökmen, B. L. Lipphardt, Jr., B. K. Haus, E. H. Ryan, A. C. Haza, et al. 2014. Submesoscale dispersion in the vicinity of the Deepwater Horizon spill, Proc. Nat. Acad. Sci., 111, 12693–12698. doi: 10.1073/pnas.1402452111.

Poulain, P.-M. 1999. Drifter observations of surface circulation in the Adriatic Sea between December 1994 and March 1996, J. Mar. Sys., *20*, 231–253. doi: 10.1016/S0924-7963(98)00084-0

Poulain, P.-M., A. Bussani, R. Gerin, R. Jungwirth, E .Mauri, M. Menna, and G. Notarstefano. 2013. Mediterranean surface currents measured with drifters: from basin to subinertial scales, Oceanography, 26, 38–47. doi: 10.5670/oceanog.2013.03

Poulain, P.-M., R. Gerin, M. Rixen, P. Zanasca, J. Teixeira, A. Griffa, et al. 2012. Aspects of the surface circulation in the Liguro-Provençal basin and Gulf of Lion as observed by satellite-tracked drifters (2007-2009), B. Geofis. Teor. Appl., *53*, 261–279.

Poulain, P.-M., M. Menna, and E. Mauri. 2012. Surface geostrophic circulation of the Mediterranean Sea derived from drifter and satellite altimeter data, J. Phys. Oceanogr., *42*, 973–990. doi: 10.1175/JPO-D-11-0159.1

Poulain, P.M., and P.P. Niiler. 1989. Statistical analysis of the surface circulation in the California current system using satellite-tracked drifters, J. Phy. Oceanogr. *19*, 1588–1603. doi: 10.1175/1520-0485(1989)019,1588:SAOTSC.2.0.CO;2

Provenzale, A. 1999. Transport by coherent barotropic vortices, J. Ann. Res. Fluid Mech., *31*, 55–93. doi: 10.1146/annurev.fluid.31.1.55

Renault, L., T. Oguz, A. Pascual, G. Vizoso, and J. Tintore. 2012. Surface circulation in the Alboran Sea (western Mediterranean) inferred from remotely sensed data, J. Geophys. Res, *117*, C08009. doi: 10.1029/2011JC007659

Richardson, L. F. 1926. Atmospheric diffusion shown on a distance neighbor graph, Philos. Trans. R. Soc. Lond. A, *110*, 709–737. doi: 10.1098/rspa.1926.0043

Sansón, L. Z. 2015. Surface dispersion in the Gulf of California, J. Prog. Oceanogr., *137*, 24–37. doi: 10.1016/j.pocean.2015.04.008

Sansón, L. Z, P. Perez-Brunius, and J. Sheinbaum. 2017. Surface relative dispersion in the southwestern Gulf of Mexico, J. Phys. Oceanogr., *47*, 387–403. doi: 10.1016/j.pocean.2015.04.008

Schroeder, K., A. C. Haza, A. Griffa, T. M. Ozgoekmen, P.-M. Poulain, R. Gerrin, et al. 2011. Relative dispersion in the Ligure-Provençal basin: from sub-mescoscale to mesoscale, J. Deep Sea Res. Part I Oceanogr. Res. Pap., *58*, 209–228. doi: 10.1016/j.dsr.2010.11.004

Sebille, E. V., S. Waterman, A. Barthel, R. Lumpkin, S. R. Keating, C. Fogwill, and C. Turney. 2015. Pairwise surface drifter separation in the western Pacific sector of the Southern Ocean, J. Geophys. Res. Oceans, *120*, 6769–6781. doi: 10.1002/2015JC010972

Sybrandy, A. L., and P. P. Niiler. 1991. WOCE/TOGA Lagrangian drifter construction manual, SIO Reference 91/6, WOCE Report No. 63. La Jolla, CA: Scripps Institution of Oceanography, 58 pp.

Taupier-Letage, I., I. Puillat, P. Raimbault, and C. Millot. 2003. Biological response to mesoscale eddies in the Algerian Basin, J. Geophys. Res., 108, C83245. doi: 10.1029/1999JC000117

Taylor, G. I. 1921. Diffusion by continuous movements, Proc. Lond. Math. Soc., *20*, 196–212. doi: 10.1112/plms/s2-20.1.196

Testor, P., U. Send, J.-C. Gascard, C. Millot, I. Taupier-Letage, and K. Beranger. 2005. The mean circulation of the southwestern Mediterranean Sea: Algerian Gyres, J. Geophys. Res., *110*, C11017. doi: 10.1029/2004JC002861

Weiss, J. 1991. The dynamics of the enstrophy transfer in two dimensional turbulence, J. Physica D, *48*, 273–294. doi: 10.1016/0167-2789(91)90088-Q

Young, W. R., P. B., Rhines, and C. J. R. Garrett. 1982. Shear-flow dispersion, internal waves and horizontal mixing in the ocean, J. Phys. Oceanogr. *12*, 515–527. doi: 10.1175/1520-0485(1982)012<0515:SFDIWA>2.0.CO;2

Received: *1 May 2018*; revised: *14 February 2019*.